

namics must be of first-order importance to their evolution (e.g. Harbor et al., 1988; Anderson et al., 2006). However, measures of subglacial dynamics, such as basal shear and normal stress, are inherently difficult to obtain owing to the general inaccessibility of the subglacial environment.

5 A few studies have measured sliding velocity and basal stress directly; under Glacier d'Argentière in the French Alps (Boulton et al., 1979) and under Engabreen in Norway (Cohen et al., 2000, 2005; Iverson et al., 2003). These studies measured shear stress values between 0.1–0.3 MPa. However, interpretations from these studies are complicated by their limited spatial and temporal extent, and by local heterogeneity such as
10 the presence of cavities. It is therefore not possible to investigate catchment-wide variations in shear stress from these empirical studies. Knowledge of spatial and temporal variations in subglacial dynamics therefore rely mostly on inversion of geophysical data (e.g. Joughin et al., 2006, 2012; Habermann et al., 2013; Morlighem et al., 2013). Despite several complications in such studies (Joughin et al., 2004; Gudmundsson and
15 Raymond, 2008; Habermann et al., 2012), and very different subglacial settings, these studies also find basal shear stress in the order of 0.1–0.4 MPa.

Numerical landscape evolution models are increasingly used to address fundamental questions relating to formation of glacial landscapes. The models can integrate erosional processes across the vast timescales of landscape evolution. This has improved
20 the understanding of glacial valley evolution (Oerlemans, 1984; Harbor et al., 1988; Anderson et al., 2006; Herman et al., 2011), hanging-valley formation (MacGregor et al., 2000), as well as mountain-range height and relief development (Kessler et al., 2008; Egholm et al., 2009; Tomkin, 2009; Pedersen and Egholm, 2013; Pedersen et al., 2014). Moreover, recent studies have investigated the importance of glacial hydrology
25 (Herman et al., 2011; Beaud et al., 2014), subglacial thermal regimes (Jamieson et al., 2008), sediment transport (Egholm et al., 2012), topographic control (Pedersen and Egholm, 2013; Pedersen et al., 2014), as well as feedbacks between different erosional processes (Braun et al., 1999; MacGregor et al., 2009; Egholm et al., 2015).

The evolution of glacial dynamics

C. F. Brædstrup et al.

Title Page

Abstract

Introduction

Conclusions

References

Tables

Figures



Back

Close

Full Screen / Esc

Printer-friendly Version

Interactive Discussion



**The evolution of
glacial dynamics**

C. F. Brædstrup et al.

Title Page

Abstract

Introduction

Conclusions

References

Tables

Figures



Back

Close

Full Screen / Esc

Printer-friendly Version

Interactive Discussion



Although often hidden by results focussing on sliding speed, basal shear stress is an important underlying factor for scaling glacial erosion. Erosion rate is commonly assumed to scale with either basal sliding speed (e.g. Oerlemans, 1984; Harbor et al., 1988; Braun et al., 1999; Tomkin, 2009; Egholm et al., 2009; Herman et al., 2011) or ice discharge (e.g. MacGregor et al., 2000, 2009; Anderson et al., 2006; Kessler et al., 2008), and both depend on subglacial stress through sliding relations. Resolving variations in basal stress under glaciers is therefore important for modelling and understanding patterns of glacial erosion.

Ice motion can be computed using the Stokes equations (Stokes, 1845), which balance the stress components in the ice under the assumption of negligible inertia. Solving the full set of Stokes equations is a computationally demanding task, and most applications therefore use computationally efficient shallow-ice approximations (Mahaffy, 1976; Hutter, 1983; Blatter, 1995; Baral et al., 2001; Pattyn, 2003; Egholm et al., 2011). However, it is well known that the accuracy of these approximations depends strongly on the aspect ratio of the ice (ice thickness vs. horizontal extent), the bed slope, and horizontal gradients in ice velocity (Hutter, 1983; Baral et al., 2001).

As an end-member approximation, the zero'th-order shallow ice approximation (SIA) is computationally very efficient, but the approximation is only considered valid for the interior parts of large ice sheets where ice surface gradients are small and smoothly varying (Hutter, 1983; Le Meur et al., 2004; Hindmarsh, 2004). The limitation of SIA models arises mainly because the approximation ignores spatial stress gradients that provide regional coupling of ice flow across a glacier. The latter drawback has led to an increased use of higher-order shallow-ice models (HOM), which are considered more accurate in cases where ice velocity vary over relatively short distances (e.g. Pattyn, 2003; Hindmarsh, 2004; Egholm et al., 2011). However, the precise relationship between the aspect ratio of the ice and the accuracy of the shallow ice approximations is only vaguely defined. As a rule of thumb, the aspect ratio should be very small ($< 10^{-2}$) for a zero'th order approximation like SIA, while it may be higher (up to 1) for a second-order shallow ice approximation (Baral et al., 2001). Thus, although the higher-order

ice dynamics of HOMs should increase accuracy compared to SIA models in steep landscapes, they too will be challenged for example when bed slopes increase beyond a certain limit. These limitations and their implications have received little attention in alpine settings, despite being of prime importance to a number of areas in glaciology and landscape evolution.

Existing benchmark studies have compared results from different models (SIA to full-Stokes models) (Hubbard, 2000; Le Meur et al., 2004; Hindmarsh, 2004; Pattyn et al., 2008; Ahlkrone et al., 2013), but all have focused on simple descriptions of three-dimensional glacial landforms, often formulated by mathematical functions. A recent study by Headley and Ehlers (2015) compared two glacial models (a SIA model and a three-dimensional full-Stokes model) in a realistic landscape and found marked differences between models. As it is vital for predictions of ice flow and subglacial erosion to resolve subglacial stress accurately, we perform new stress benchmark experiments on a synthetic but realistic three-dimensional fluvial landscape using both the iSOSIA higher-order model and the Elmer/ICE full-Stokes model (Sect. 2.3). While this setup prevents analytical solution of the Stokes equations, it allows us to compare the iSOSIA approximation to a full-Stokes computational model in a realistic setting under different scales of relief (Sects. 3.1 and 3.2).

In subsequent experiments, the same fluvial landscape provides the basis for iSOSIA experiments that combine subglacial erosion with different models for basal sliding (Sect. 3.3). These final experiments are designed to explore long-term feedbacks between landscape evolution and subglacial dynamics.

2 Methods

In the following we introduce the ice models used in this study, along with technical details on experimental setup and model comparison.

The evolution of glacial dynamics

C. F. Brædstrup et al.

Title Page

Abstract

Introduction

Conclusions

References

Tables

Figures



Back

Close

Full Screen / Esc

Printer-friendly Version

Interactive Discussion



2.1 Elmer/ICE

The Elmer multi-physics software package (www.csc.fi/elmer) provides a finite-element framework for modelling both linear and non-linear three-dimensional flow problems. The Elmer software is developed at CSC in Finland with collaborators around the world, and is published under a GNU Public License (GPL). A special edition of Elmer, named Elmer/ICE, is available with algorithms designed especially for problems related to ice flow (Gagliardini et al., 2013).

Elmer/ICE provides a highly accurate description of glacial dynamics by solving the full set of Stokes equations in three dimensions. However, the high degree of accuracy comes with a very high computational demand. Elmer is developed to run very efficiently in parallel (Gagliardini et al., 2013) to reduce computation time significantly, but the computations performed here still required at least two to three orders of magnitude more time than the corresponding SIA and iSOSIA simulations. Owing to the high computational demand, we only use Elmer/ICE to perform steady-state simulations without erosion.

2.2 iSOSIA

iSOSIA has been developed specifically for modelling glacial landscape evolution (Egholm et al., 2011). The ice model includes all stress components of the Stokes equations. However, by using a second-order shallow ice approximation (Baral et al., 2001) iSOSIA represents a computationally efficient alternative to full-Stokes models. The main limiting assumption in iSOSIA is that horizontal, longitudinal and transverse stress components are not allowed to vary with depth in the ice. This assumption facilitates analytical depth-integration of velocities, and iSOSIA is hence a depth-integrated two-dimensional model.

The iSOSIA equations are highly non-linear because components of stress and ice velocity are connected through the non-Newtonian Glen's flow law for ice with a stress exponent of 3. The non-linear equations are relaxed using an iterative Red-Black finite-

ESURFD

3, 1143–1178, 2015

The evolution of glacial dynamics

C. F. Brædstrup et al.

Title Page

Abstract

Introduction

Conclusions

References

Tables

Figures

◀

▶

◀

▶

Back

Close

Full Screen / Esc

Printer-friendly Version

Interactive Discussion



difference Gauss–Seidel method (Briggs et al., 2000). iSOSIA was also recently ported to graphical processing units (GPU) with increased computational efficiency (Brædstrup et al., 2014).

2.3 Experimental Setup

5 All experiments are performed on a synthetic topography generated using a fluvial landscape evolution model based on stream-power erosion (Fig. 1a; Braun and Sambridge, 1997). This provides a particularly convenient setup where the uppermost drainage divide follows the grid boundaries, avoiding ice flow out of the model domain. The fluvial landscape has V-shaped valleys and concave longitudinal valley profiles that drain the
 10 landscape from a maximum elevation of 2500 m above sea-level down to 0 m (Fig. 1a). The computational grid is 20 by 40 km, consisting of 100 by 200 cells (i.e. 200 m resolution).

Ice thickness is time-integrated using the continuity equation,

$$\frac{\partial H}{\partial t} = -\nabla \times \mathbf{q} + M, \quad (1)$$

15 where H is ice thickness, t is time, \mathbf{q} is ice flux, and M is the rate of ice accumulation/ablation.

Accumulation and ablation is modelled as a simple linear function of atmospheric temperature:

$$M(x, y) = \begin{cases} -m_{\text{acc}} T(x, y), & \text{if } T(x, y) \leq 0, \\ -m_{\text{abl}} T(x, y), & \text{if } T(x, y) > 0, \end{cases} \quad (2)$$

20 where

$$T(x, y) = T_{\text{sl}} - dT_h h(x, y) \quad (3)$$

Title Page

Abstract

Introduction

Conclusions

References

Tables

Figures

◀

▶

◀

▶

Back

Close

Full Screen / Esc

Printer-friendly Version

Interactive Discussion



is the atmospheric temperature. T_{sl} is the sea-level temperature, dT_h is the lapse rate, and h is bedrock elevation above sea level. m_{acc} is the accumulation gradient and m_{abl} is the ablation gradient. All values are listed in Table 1.

Experiments 1 and 2 assume steady state, and use the continuity equation only to construct the ice surface configuration (Fig. 1b). In experiment 3 the continuity equation is used to update ice thickness throughout transient simulations. However, in order to avoid that feedbacks between mass-balance and topography influence the subglacial stress distribution, we fix the mass balance in time and ignore the influence of topographical change on accumulation and ablation. This allows us to more clearly study the direct influence of the evolving bed topography on subglacial stress under conditions of constant ice flux.

Ice creep and basal sliding contribute to the ice flux vector, \mathbf{q} , in Eq. (1). The rate of ice creep is governed by Glen's flow law:

$$\dot{\epsilon}_{ij} = A\tau_e^{n-1} s_{ij}, \quad (4)$$

where $\dot{\epsilon}_{ij}$ is the deviatoric strain rate tensor and s_{ij} is the deviatoric stress tensor. A and n are ice flow parameters (Table 1), and τ_e is the effective stress:

$$\tau_e = \sqrt{s_{xz}^2 + s_{yz}^2 + s_{xy}^2 + \frac{1}{2}(s_{xx}^2 + s_{yy}^2 + s_{zz}^2)}, \quad (5)$$

iSOSIA uses a depth-integrated version of Glen's flow law to compute the depth-averaged flow velocities (Egholm et al., 2011).

The benchmarking experiments 1 and 2 use a simple Weertman sliding relation to relate basal shear stress to the rate of subglacial sliding. In experiment 3, however, we make use of three different sliding relations to examine the sensitivity of subglacial stress to first-order assumptions on basal sliding velocity. The three sliding models are

Title Page

Abstract

Introduction

Conclusions

References

Tables

Figures

◀

▶

◀

▶

Back

Close

Full Screen / Esc

Printer-friendly Version

Interactive Discussion



all represented by relations between basal shear stress and sliding velocity:

$$\text{Weertman sliding: } \tau_s^2 = u_s / C_s \quad (\text{Weertman, 1957}) \quad (6)$$

$$\text{Empirical sliding: } \tau_s^2 = u_s N / C_s \quad (\text{Budd et al., 1979}) \quad (7)$$

$$\text{Columb-friction: } \tau_s / N = C_s \left(\frac{u_s / N^n}{u_s / N^n + \lambda_0} \right)^{1/n} \quad (\text{Schoof, 2005; Gagliardini et al., 2007}) \quad (8)$$

5 Here τ_s is basal shear stress, C_s is a sliding coefficient specific to each individual relation (Table 1), u_s is basal sliding velocity, and λ_0 is a constant defining the overall bed geometry (Schoof, 2005; Gagliardini et al., 2007). The effective pressure, $N = t_n - \rho_w$, is the difference between the ice-bed normal stress, t_n , and water pressure, ρ_w . The two latter sliding relations (the empirical sliding model and Columb-friction), which are
10 both used in experiment 3, depend on effective pressure and hence subglacial water pressure. However, in order to focus on first-order correlations between topography and subglacial shear stress, we simplify the influence of hydrology and assume that water pressure is everywhere 80 % of the ice overburden pressure, $\rho_w = 0.8\rho_i gH$. We note, however, that more complex distributions of melt-water pressure may potentially affect
15 patterns of subglacial shear stress through the influence of sliding (e.g. Flowers and Clarke, 2002; Werder et al., 2013; Beaud et al., 2014). Yet, such effects are beyond the scope of the present study.

In experiment 3 the glacier erodes its bed according to the following sliding-based erosion law:

$$\dot{e} = K_a |\mathbf{u}_s|^m, \quad (9)$$

where \dot{e} is erosion rate perpendicular to the bed, K_a is the erosion constant (Table 1), m is the erosion exponent and \mathbf{u}_s is sliding velocity. Parameters governing subglacial erosion through abrasion and sliding are still being debated, and it is particularly relevant

Title Page

Abstract

Introduction

Conclusions

References

Tables

Figures

◀

▶

◀

▶

Back

Close

Full Screen / Esc

Printer-friendly Version

Interactive Discussion



The evolution of glacial dynamics

C. F. Brædstrup et al.

Title Page

Abstract

Introduction

Conclusions

References

Tables

Figures

I◀

▶I

◀

▶

Back

Close

Full Screen / Esc

Printer-friendly Version

Interactive Discussion



to question how well the sliding-based law represents subglacial quarrying (Iverson, 2012). However, sliding-based erosions laws have been shown by models to produce realistic glacial landforms (Harbor, 1992; Seddik et al., 2005; Pedersen et al., 2014), which is why we use it here to study how transformation of a landscape from fluvial-style to glacial-style influences the patterns of subglacial shear stress. Our use of the above erosion law is thus motivated more by phenomenological arguments than empirical evidence. We perform all erosional experiments with both a linear ($m = 1$) and non-linear ($m = 2$) model in order to evaluate the robustness of our conclusions.

2.4 Comparing the output of iSOSIA and Elmer/ICE

To ensure comparability between results produced by iSOSIA and Elmer/ICE, both models operate on the same synthetic input topography, represented by a rectangular grid with specified bed elevation in each grid cell. The iSOSIA solver operates directly on this two-dimensional grid, whereas for Elmer/ICE the two-dimensional grid is expanded to a full three-dimensional mesh with five vertical levels. This gridding approach ensures that both models use exactly the same topographic input and mesh topology, except for Elmer/ICE having the additional vertical layering. In order to compare ice dynamics on exactly the same ice configuration, a steady-state ice distribution is generated using iSOSIA and subsequently used by both models. A free slip boundary condition is implemented along grid edges, and isothermal conditions are assumed everywhere in the grid.

Since Elmer/ICE computes stress and velocity on a three-dimensional grid, post-processing is necessary in order to compare with iSOSIA. Horizontal stress and flow components from Elmer/ICE are therefore depth-averaged using the following function:

$$\bar{u} = \frac{1}{H} \int_0^H u(z) dz, \quad (10)$$

where u is the variable of interest (stress or velocity component), z is depth below the ice surface and H is local ice thickness.

Both models compute basal shear stress as:

$$\boldsymbol{\tau}_s = \boldsymbol{\sigma}_b \times \mathbf{n}_b - \boldsymbol{\sigma}_n, \quad (11)$$

5 where $\boldsymbol{\sigma}_b$ is the Cauchy stress tensor at the bed, and $\boldsymbol{\sigma}_n$ is the stress vector perpendicular to the bed:

$$\boldsymbol{\sigma}_n = (\mathbf{n}_b \times \boldsymbol{\sigma}_b \times \mathbf{n}_b) \mathbf{n}_b, \quad (12)$$

\mathbf{n}_b is the normal vector at the bed:

$$\mathbf{n}_b = \frac{1}{\ell_b} \left[\frac{\partial b}{\partial x}, \frac{\partial b}{\partial y}, -1 \right], \quad (13)$$

10 with

$$\ell_b = \sqrt{1 + \left(\frac{\partial b}{\partial x} \right)^2 + \left(\frac{\partial b}{\partial y} \right)^2}. \quad (14)$$

In order to provide a frame of reference, we also compare the basal shear stress of iSOSIA and Elmer/ICE to the driving-stress approximation, which is used as a proxy for basal shear stress in zero'th order shallow ice approximations (Cuffey and Paterson, 2010). The driving stress is computed as,

$$\tau_{\text{SIA}} = \rho_i g H \sqrt{\left(\frac{\partial h}{\partial x} \right)^2 + \left(\frac{\partial h}{\partial y} \right)^2}, \quad (15)$$

where ρ_i is ice density, g is gravitational acceleration, H is ice thickness and h is the elevation of the ice surface.

The evolution of glacial dynamics

C. F. Brædstrup et al.

Title Page

Abstract

Introduction

Conclusions

References

Tables

Figures

◀

▶

◀

▶

Back

Close

Full Screen / Esc

Printer-friendly Version

Interactive Discussion



3 Results

3.1 Experiment 1 – benchmarking steady-state solutions

The first two experiments are used to benchmark stress and velocity components from iSOSIA against those from Elmer/ICE. The steady-state ice configuration, which is first computed by iSOSIA and then used as input for both models, includes a main trunk glacier fed by several smaller tributary glaciers (Fig. 1b). Ice thickness reaches a maximum of 700 m in the main valley, and thins towards the glacier front and upwards in the tributaries. The depth-averaged creep velocity is highest where the ice is thickest in the main valley, reaching levels of 120 m yr^{-1} (Fig. 1d). Basal sliding speed is high in the main valley and in the steeper parts of the high tributaries (Fig. 1c).

In experiment 1, the spatial distribution of stress is characterised by similar large-scale patterns in iSOSIA and Elmer/ICE (Fig. 2a). The components of horizontal normal stress, \bar{s}_{xx} and \bar{s}_{yy} , are generally positive at high elevations, which reflects an overall extensional stress state in the accumulation zones. In the trunk valley at lower elevations, both stress components are in places negative (compressive) due to local deceleration of the ice. The latter tendency is however clearly affected by the details of the bed topography. The horizontal shear stress, \bar{s}_{xy} , is large, although of opposite sign, along both sides of the main valley due to a strong velocity gradient perpendicular to the main flow direction.

Differences between horizontal differential stress (\bar{s}_{xx} , \bar{s}_{yy} , and \bar{s}_{xy}) in Elmer/ICE and iSOSIA are in general below $\pm 0.03 \text{ MPa}$ in tributary valleys and $\pm 0.01 \text{ MPa}$ in the main valley (Fig. 2a, right column).

The basal shear stress is up to 0.2 MPa under the ice in the main trunk valley and near the tributary headwalls. Between these areas, basal shear stress is rather uniform at levels around 0.1 MPa . Differences between Elmer/ICE and iSOSIA are of order 0.025 MPa but up to 0.05 MPa in few areas (mostly along ice margins).

Sliding velocities are also similar in both models: $\sim 40 \text{ m yr}^{-1}$ in the trunk valley and around 20 m yr^{-1} in the tributaries. Yet, the Elmer/ICE solution contains areas with high-

Title Page

Abstract

Introduction

Conclusions

References

Tables

Figures

◀

▶

◀

▶

Back

Close

Full Screen / Esc

Printer-friendly Version

Interactive Discussion



frequency variations in basal sliding and shear stress, which are absent in the iSOSIA result. These areas correlate with larger differences in sliding velocity between the two models (Fig. 2c, right column).

To aid the comparison between iSOSIA and Elmer/ICE we extract stress and velocity components along two profiles in the transverse and longitudinal directions of the valley (Fig. 3). The profile A-B runs directly across the main valley, while the profile C-D starts at high elevation and follows the ice drainage along the main valley down to sea-level.

The three horizontal stress components (\bar{s}_{xx} , \bar{s}_{yy} and \bar{s}_{xy}) are all of order ± 0.04 MPa along the profiles, but vary in ways that reflect the bed topography. In the transverse direction (profile A-B, left panels of Fig. 3), stress components generally change sign in response to how the velocity components u_x and u_y vary across the valley (Fig. 1). The basal shear stress, along the same profile, is 2 to 4 times greater in magnitude than the horizontal stress components, which reflects the influence of pressure, p , as well as the vertical shear stress components s_{xz} and s_{yz} .

Along the longitudinal profile (c and d, right panels in Fig. 3), the stress components also fluctuate around zero. A clear anti-correlation exists between \bar{s}_{xx} and \bar{s}_{yy} , which indicate horizontal pure shear deformation in response to inflow of ice from the tributaries (Fig. 2a). The basal shear stress is remarkable constant along the profile and decreases only slightly up-glacier. This may seem surprising as bed slope increases significantly up-glacier. However, the effect of bed slope seems in this case to be counteracted by ice thinning.

There are no clear trends in misfit between iSOSIA and Elmer/ICE and the two models generally predict the same patterns and magnitude of stress. Again, the main difference between results is that high-frequency stress variations are slightly larger for Elmer/ICE than for iSOSIA, particularly so for the basal shear stress (Figs. 2b and 3). As expected, the SIA driving stress is generally higher, and show more intense variation, than the basal shear stress for both iSOSIA and Elmer/ICE.

The evolution of glacial dynamics

C. F. Brædstrup et al.

Title Page

Abstract

Introduction

Conclusions

References

Tables

Figures



Back

Close

Full Screen / Esc

Printer-friendly Version

Interactive Discussion



3.2 Experiment 2 – the effect of relief

In the second experiment we gradually increase the total relief of the fluvial landscape to test how this influences the consistency between iSOSIA and Elmer/ICE results. Theoretically, increasing the relief should decrease the accuracy of iSOSIA as bed gradients and spatial variations in flow velocity intensify.

We use a simple scaling of the fluvial topography from experiment 1 in order to systematically increase the relief without affecting the drainage patterns (Fig. 4c). We then run iSOSIA to a steady-state ice configuration for all amplified topographies and transfer the resulting ice thicknesses to Elmer/Ice in order to compute stress and velocity components under similar conditions.

When up-scaling relief, the ice-creep velocity increases significantly, the glacier thins, and its front margin advances (Fig. 4a). Because the ice-flow velocity is amplified almost uniformly, the magnitude of the horizontal stress components, which reflect local velocity gradients, also increase in response to the larger relief (Fig. 5). All three stress components still vary around 0 MPa, but the amplitude of the variation increases with relief. The largest response in horizontal stress due to increased relief, occurs in the steep high-elevation areas near the headwalls.

In contrast to the englacial horizontal stress, the basal shear stress is remarkably unaffected by the increasing relief and remains rather uniform around 0.1–0.2 MPa for all four situations (Fig. 5).

Examining differences between Elmer/ICE and iSOSIA, we note that both models agree on regional stress patterns and that iSOSIA stress follows the Elmer/ICE solution reasonably well across the range of reliefs tested here. The regional misfit remains small even when maximum relief is 6250 m (Fig. 5c). There are however areas where the comparison exposes an increasing misfit between iSOSIA and Elmer/ICE, particularly when focussing on variations at length scales of a few hundred meters. These areas are mainly associated with thin ice and steep ice-surface topography near the glacial terminus or the headwall areas.

ESURFD

3, 1143–1178, 2015

The evolution of glacial dynamics

C. F. Brædstrup et al.

Title Page

Abstract

Introduction

Conclusions

References

Tables

Figures

◀

▶

◀

▶

Back

Close

Full Screen / Esc

Printer-friendly Version

Interactive Discussion



The evolution of glacial dynamics

C. F. Brædstrup et al.

Title Page

Abstract

Introduction

Conclusions

References

Tables

Figures



Back

Close

Full Screen / Esc

Printer-friendly Version

Interactive Discussion



Unlike the basal shear stress from iSOSIA and Elmer/ICE, both regional and local variations of SIA driving stress increase significantly with relief (Fig. 5, blue line). While the misfit between Elmer/ICE and iSOSIA are in the order of 0–0.05 MPa for a relief of 5000 m (with spikes up to 0.1 MPa), the misfit between SIA and Elmer/ICE quickly reaches levels well above 0.2 MPa. This misfit is caused by the driving stress' lack of sensitivity to regional velocity variations as well as bed topography.

3.3 Experiment 3 – evolution of stress under glacial erosion

After evaluating steady-state solutions of iSOSIA against Elmer/ICE we now investigate the long-term transient evolution of basal shear stress in response to subglacial erosion and landscape development. We only use iSOSIA for this experiment as the computational costs of Elmer/ICE prevents us from running simulations over the thousand year timescales required for glacial landscape development. The initial topography from experiment 1 is used as input for iSOSIA and is slowly eroded using a sliding-based erosion law (Eq. 9).

First, we run the experiment using the Weertman relation for sliding (Eq. 6; Weertman, 1957) in combination with a non-linear erosion law ($m = 2$ in Eq. 9). We find that the V-shaped fluvial valley structure is transformed into a wider and steep-sided U-shaped trough (Fig. 6). This is in agreement with previous studies (Harbor, 1992; Seddik et al., 2005; Egholm et al., 2012). Several other characteristic glacial landforms also appear as a result of glacial erosion, including steep and narrow upper ridges, flattened valley floors, hanging valleys and truncated spurs.

As expected, bed slopes increase in many areas of the landscape, particularly along valley sides and near headwalls (Fig. 7). However, along the longitudinal flowline of the glacier, bed slopes generally decrease as glacial erosion flattens the valley floor and removes bedrock features that obstruct flow. This development generally cause bed shear stress to decrease in amplitude and become more uniformly distributed under the ice (Fig. 7). This reduction in basal shear stress also decreases sliding velocity as a result of the Weertman sliding relation (Eq. 6; Fig. 7).

The evolution of glacial dynamics

C. F. Brædstrup et al.

Title Page

Abstract

Introduction

Conclusions

References

Tables

Figures



Back

Close

Full Screen / Esc

Printer-friendly Version

Interactive Discussion



same bed topography and ice distribution, as well as the same horizontal grid structure (with an additional vertical grid-dimension for Elmer/ICE). We note here that the true accuracy of both methods is expected to depend on grid resolution. For example, the finite-element method in Elmer/ICE allows irregular grid structures that may increase the computational accuracy, e.g. along ice margins where steep ice surface gradients call for increased spatial resolution (Durand et al., 2011). However, a comparison study designed to uncover the difference caused by various approximations to the Stokes equations is not meaningful if similar meshes are not used.

The benchmark experiments show that iSOSIA and Elmer/ICE predict the same overall patterns of stress and velocity. In both models, components of horizontal stress and stress gradients interact with flow patterns on a regional scale (i.e. across topographical gradients, which is in strong contrast to the driving stress in SIA models). This highlights, in accordance with previous studies (e.g. Le Meur et al., 2004; Hindmarsh, 2004; Egholm et al., 2011, 2012), the benefits of HOM and full-Stokes models over SIA models. The main difference in results from iSOSIA and Elmer/ICE seems to be confined to spatial scales of few hundred meters (i.e. the grid cell spacing). In particular, Elmer/ICE includes high-frequency fluctuations in basal shear stress and sliding (Fig. 2) whereas the iSOSIA results appear more smoothly varying. The smoother pattern in iSOSIA is perhaps not surprising when considering the inherent depth-integration of horizontal stress. On the other hand, the relatively large differences in sliding velocity between neighbouring grid cells in Elmer/ICE are surprising and cannot easily be explained by variations in bed topography.

The high-frequency variations of Elmer/ICE are amplified slightly when the total catchment relief increase from 2500 to 7500 m (Fig. 5). On the other hand, the more regional accordance between iSOSIA and Elmer/ICE stress predictions seems almost unaffected by the increasing relief. This is in contrast to the SIA driving stress, which rises with increasing relief.

4.2 The evolution of stress in response to erosion

The iSOSIA simulations with erosion (experiment 3) suggest that variations in basal shear stress are generally reduced by the gradual transformation from a fluvial to a glacial topography. We observe this trend for all sliding laws tested in this study (Weertmann, empirical, Columb-friction; Fig. 8) and for two different sliding exponents in the erosion law.

The highest initial levels of basal shear stress are associated with bends in the fluvial channel profile that forms interlocking spurs (Fig. 7). These spurs are truncated by glacial erosion which decreases basal shear stress. In the main valley, glacial erosion thereby efficiently remove obstacles and straightens the path of ice flow. In addition to this, glacial erosion flattens the longitudinal valley profile and widens its cross section, which also contributes to reduced basal shear stress (Harbor, 1992; Seddik et al., 2005).

It is not surprising in the current study, that the modelled glacial erosion primarily attacks portions of the glacial bed where basal shear stress is high. Basal shear stress is connected to sliding rate through the sliding relations (Eqs. 6–8), which, in turn, is assumed to scale rates of erosion (Eq. 9). We note that different rules for glacial erosion, for example the ones based on mechanics of bedrock quarrying (Iverson, 2012), could depend differently on sliding and shear stress. Feedbacks between stress and erosion might be different in such cases. On the other hand, the experiments presented here result in topographic features that resembles well-known glacial landforms, and it seems reasonable that smoother and flatter post-glacial landforms are associated with less drag from the ice.

With increased erosion, the resulting decrease in basal shear stress leads in our experiment to a lowering of sliding rate, and hence slowdown of erosion. This is a direct consequence of the sliding relations used. Two of the sliding relations have a power-law scaling between stress and sliding, and sliding must decrease with decreasing shear stress (the Weertman and the empirical sliding relations). The Coulomb-friction

ESURFD

3, 1143–1178, 2015

The evolution of glacial dynamics

C. F. Brædstrup et al.

Title Page

Abstract

Introduction

Conclusions

References

Tables

Figures



Back

Close

Full Screen / Esc

Printer-friendly Version

Interactive Discussion



The evolution of glacial dynamics

C. F. Brædstrup et al.

Title Page

Abstract

Introduction

Conclusions

References

Tables

Figures



Back

Close

Full Screen / Esc

Printer-friendly Version

Interactive Discussion



sliding model, on the other hand, operates with an upper limit to the bed's ability to support shear stress (the bed resistance). In addition to the sliding rate, the upper stress limit (the bed resistance) associated with Coulomb-friction depends on water pressure and the bed roughness, which is controlled by parameters C_s and λ_0 in Eq. (8). Here we speculate, that if the bed resistance decreases more rapidly than the shear stress imposed on the bed by the ice flow, then sliding may possibly accelerate as the topography is eroded in contrast to the results presented here. The bed resistance could decrease if, for example, the bed is smoothed by erosion or if the flatter glacial longitudinal valley profile reduces the melt-water drainage efficiency of the glacier. Our experiment 3 does not show such behaviour, partly because we ignore effects of melt-water hydrology, and partly because the parameters representing bed roughness (C_s and λ_0 in Eq. 8) are treated as constants independent of erosion. However, understanding how glacial erosion affects the topographical conditions that promote cavitation on length scales below the current grid resolution of landscape evolution models, may be important for advancing our understanding of feedbacks between glacial dynamics and topographical development.

Because of general lowering of basal shear stress with erosion, our results support the hypothesis that glacial erosion is most efficient in the initial phase of glacial landscape evolution, when landforms are unadapted to the new glacial regime (Harbor, 1992; Braun et al., 1999). In general, however, landscape evolution is influenced by several processes not accounted here, such as a transient climate forcing (Pedersen and Egholm, 2013), changing topography due to a tectonic forcing (e.g. Tomkin and Braun, 2002), periglacial processes acting in concert with glacial erosion (e.g. Egholm et al., 2015), fluvial processes and mass wasting affecting the landscape especially during ice-free interglacial periods (e.g. Schlunegger and Hinderer, 2003), and subglacial fracturing in response to high differential in situ stresses (e.g. Leith et al., 2014).

5 Conclusions

We have investigated and compared the spatial distribution of subglacial shear stress in both a higher-order shallow-ice model (iSOSIA) and a full-Stokes three-dimensional model (Elmer/ICE). Using iSOSIA only, we also investigated the temporal evolution of basal shear stress in response to subglacial erosion. In total, we conducted three experiments in order to resolve different aspects of subglacial shear stress. We found that,

- iSOSIA and Elmer/ICE produce stress and sliding patterns that are largely similar under the conditions tested.
- In the alpine setting used here, basal shear stress seems rather insensitive to increases in overall relief, as reduction on ice thickness counteracts the effects of bed steepening. Thus, increasing total relief by a factor 3 only produces a small response in basal shear stress.
- Subglacial erosion removes obstacles that give rise to high basal shear stress in the pre-glacial landscape setting. By this, glacial erosion leads to lower and more uniformly distributed basal shear stress.
- Using three different sliding relations and two different erosion laws, we find a stabilising feedback between basal shear stress, sliding, erosion, and topography. This feedback depends however on constant sliding coefficients, which in a more realistic setting could be altered by long-term changes to the bed roughness.

Author contributions. C. F. Brædstrup and D. L. Egholm designed the study, developed the computational tools and conducted iSOSIA experiments. C. F. Brædstrup was responsible for work with Elmer/ICE. C. F. Brædstrup prepared the manuscript with contributions from all co-authors.

Acknowledgements. We thank Thomas Zwinger from the Elmer/ICE team for invaluable help with initial model setup. This research was funded by The Danish Council for Independent Research under the Sapere Aude program.

Title Page

Abstract

Introduction

Conclusions

References

Tables

Figures



Back

Close

Full Screen / Esc

Printer-friendly Version

Interactive Discussion



References

- Ahlkrona, J., Kirchner, N., and Lötstedt, P.: Accuracy of the zeroth- and second-order shallow-ice approximation – numerical and theoretical results, *Geosci. Model Dev.*, 6, 2135–2152, doi:10.5194/gmd-6-2135-2013, 2013. 1147
- 5 Anderson, R. S., Molnar, P., and Kessler, M. A.: Features of glacial valley profiles simply explained, *J. Geophys. Res.-Earth*, 111, F01004, doi:10.1029/2005JF000344, 2006. 1145, 1146
- Baral, D. R., Hutter, K., and Greve, R.: Asymptotic theories of large-scale motion, temperature, and moisture distribution in land-based polythermal ice sheets: a critical review and new developments, *Appl. Mech. Rev.*, 54, 215–256, 2001. 1146, 1148
- 10 Beaud, F., Flowers, G. E., and Pimentel, S.: Seasonal-scale abrasion and quarrying patterns from a two-dimensional ice-flow model coupled to distributed and channelized subglacial drainage, *Geomorphology*, 219, 176–191, 2014. 1145, 1151
- Blatter, H.: Velocity and stress fields in grounded glaciers: a simple algorithm for including deviatoric stress gradients, *J. Glaciol.*, 41, 333–344, 1995. 1146
- 15 Boulton, G., Morris, E., Armstrong, A., and Thomas, A.: Direct measurement of stress at the base of a glacier, *J. Glaciol.*, 22, 3–24, 1979. 1145
- Braun, J. and Sambridge, M.: Modelling landscape evolution on geological time scales: a new method based on irregular spatial discretization, *Basin Res.*, 9, 27–52, doi:10.1046/j.1365-2117.1997.00030.x, 1997. 1149
- 20 Braun, J., Zwartz, D., and Tomkin, J.: A new surface-processes model combining glacial and fluvial erosion, *Ann. Glaciol.*, 28, 282–290, 1999. 1145, 1146, 1161
- Brædstrup, C. F., Damsgaard, A., and Egholm, D. L.: Ice-sheet modelling accelerated by graphics cards, *Comput. Geosci.*, 72, 210–220, doi:10.1016/j.cageo.2014.07.019, 2014. 1149
- 25 Briggs, W. L., Henson, V. E., and McCormick, S. F.: *A Multigrid Tutorial*, SIAM, Philadelphia, PA, USA, 2000. 1149
- Budd, W. F., Keage, P. L., and Blundy, N. A.: Empirical studies of ice sliding, *J. Glaciol.*, 23, 157–170, 1979. 1158
- Cohen, D., Hooke, R. L., Iverson, N. R., and Kohler, J.: Sliding of ice past an obstacle at Engabreen, Norway, *J. Glaciol.*, 46, 599–610, 2000. 1145
- 30

The evolution of glacial dynamics

C. F. Brædstrup et al.

Title Page

Abstract

Introduction

Conclusions

References

Tables

Figures



Back

Close

Full Screen / Esc

Printer-friendly Version

Interactive Discussion



The evolution of glacial dynamics

C. F. Brædstrup et al.

Title Page

Abstract

Introduction

Conclusions

References

Tables

Figures

I◀

▶I

◀

▶

Back

Close

Full Screen / Esc

Printer-friendly Version

Interactive Discussion



Cohen, D., Iverson, N., Hooyer, T., Fischer, U., Jackson, M., and Moore, P.: Debris-bed friction of hard-bedded glaciers, *J. Geophys. Res.-Earth*, 110, F02007, doi:10.1029/2004JF000228, 2005. 1145

Cuffey, K. M. and Paterson, W.: *The Physics of Glaciers*, 4th edn., Academic Press, Burlington, Massachusetts, USA, 2010. 1153

Durand, G., Gagliardini, O., Favier, L., Zwinger, T., and le Meur, E.: Impact of bedrock description on modeling ice sheet dynamics, *Geophys. Res. Lett.*, 38, L20501, doi:10.1029/2011GL048892, 2011. 1159

Egholm, D. L., Nielsen, S. B., Pedersen, V. K., and Lesemann, J.-E.: Glacial effects limiting mountain height, *Nature*, 460, 884–887, 2009. 1145, 1146

Egholm, D. L., Knudsen, M. F., Clark, C. D., and Lesemann, J. E.: Modeling the flow of glaciers in steep terrains: The integrated second-order shallow ice approximation (iSOSIA), *J. Geophys. Res.-Earth*, 116, F02012, doi:10.1029/2010JF001900, 2011. 1146, 1148, 1150, 1159

Egholm, D., Pedersen, V., Knudsen, M., and Larsen, N.: On the importance of higher order ice dynamics for glacial landscape evolution, *Geomorphology*, 141–142, 67–80, 2012. 1145, 1157, 1159

Egholm, D. L., Andersen, J. L., Knudsen, M. F., Jansen, J. D., and Nielsen, S. B.: The periglacial engine of mountain erosion – Part 2: Modelling large-scale landscape evolution, *Earth Surf. Dynam. Discuss.*, 3, 327–369, doi:10.5194/esurf-d-3-327-2015, 2015. 1145, 1161

Evans, I. S. and McClean, C. J.: The land surface is not unifractal; variograms, cirque scale and allometry, *Z. Geomorphol.*, 101, 127–147, 1995. 1144

Flowers, G. E. and Clarke, G. K. C.: A multicomponent coupled model of glacial hydrology., 1. Theory and synthetic examples, *J. Geophys. Res.-Sol. Ea.*, 107, ECV 9–1–17, doi:10.1029/2001JB001122, 2002. 1151

Gagliardini, O., Cohen, D., Råback, P., and Zwinger, T.: Finite-element modeling of subglacial cavities and related friction law, *J. Geophys. Res.-Earth*, 112, F02027, doi:10.1029/2006JF000576, 2007. 1151, 1158

Gagliardini, O., Zwinger, T., Gillet-Chaulet, F., Durand, G., Favier, L., de Fleurian, B., Greve, R., Malinen, M., Martín, C., Råback, P., Ruokolainen, J., Sacchetti, M., Schäfer, M., Seddik, H., and Thies, J.: Capabilities and performance of Elmer/Ice, a new-generation ice sheet model, *Geosci. Model Dev.*, 6, 1299–1318, doi:10.5194/gmd-6-1299-2013, 2013. 1148

The evolution of glacial dynamics

C. F. Brædstrup et al.

Title Page

Abstract

Introduction

Conclusions

References

Tables

Figures



Back

Close

Full Screen / Esc

Printer-friendly Version

Interactive Discussion



- Gudmundsson, G. H. and Raymond, M.: On the limit to resolution and information on basal properties obtainable from surface data on ice streams, *The Cryosphere*, 2, 167–178, doi:10.5194/tc-2-167-2008, 2008. 1145
- Habermann, M., Maxwell, D., and Truffer, M.: Reconstruction of basal properties in ice sheets using iterative inverse methods, *J. Glaciol.*, 58, 795–807, 2012. 1145
- Habermann, M., Truffer, M., and Maxwell, D.: Changing basal conditions during the speed-up of Jakobshavn Isbræ, Greenland, *The Cryosphere*, 7, 1679–1692, doi:10.5194/tc-7-1679-2013, 2013. 1145
- Harbor, J. M.: Numerical modeling of the development of U-shaped valleys by glacial erosion, *Geol. Soc. Am. Bull.*, 104, 1364–1375, 1992. 1152, 1157, 1160, 1161
- Harbor, J. M., Hallet, B., and Raymond, C. F.: A numerical model of landform development by glacial erosion, *Nature*, 333, 347–349, doi:10.1038/333347a0, 1988. 1145, 1146
- Headley, R. M. and Ehlers, T. A.: Ice flow models and glacial erosion over multiple glacial–interglacial cycles, *Earth Surf. Dynam.*, 3, 153–170, doi:10.5194/esurf-3-153-2015, 2015. 1147
- Herman, F., Beaud, F., Champagnac, J.-D., Lemieux, J.-M., and Sternai, P.: Glacial hydrology and erosion patterns: A mechanism for carving glacial valleys, *Earth Planet. Sc. Lett.*, 310, 498–508, 2011. 1145, 1146
- Hindmarsh, R. C. A.: A numerical comparison of approximations to the Stokes equations used in ice sheet and glacier modeling, *J. Geophys. Res.-Earth*, 109, F01012, doi:10.1029/2003JF000065, 2004. 1146, 1147, 1159
- Hubbard, A.: The verification and significance of three approaches to longitudinal stresses in high-resolution models of glacier flow, *Geogr. Ann. A*, 82, 471–487, 2000. 1147
- Hutter, K.: *Theoretical Glaciology: Material Science of Ice and the Mechanics of Glaciers and Ice Sheets*, Springer, New York, USA, 1983. 1146
- Iverson, N. R.: A theory of glacial quarrying for landscape evolution models, *Geology*, 40, 679–682, doi:10.1130/G33079.1, 2012. 1152, 1160
- Iverson, N. R., Cohen, D., Hooyer, T. S., Fischer, U. H., Jackson, M., Moore, P. L., Lappégard, G., and Kohler, J.: Effects of basal debris on glacier flow, *Science*, 301, 81–84, 2003. 1145
- Jamieson, S. S. R., Hulton, N. R. J., and Hagdorn, M.: Modelling landscape evolution under ice sheets, *Geomorphology*, 97, 91–108, 2008. 1145

The evolution of glacial dynamics

C. F. Brædstrup et al.

Title Page

Abstract

Introduction

Conclusions

References

Tables

Figures



Back

Close

Full Screen / Esc

Printer-friendly Version

Interactive Discussion



- Joughin, I., MacAyeal, D. R., and Tulaczyk, S.: Basal shear stress of the Ross ice streams from control method inversions, *J. Geophys. Res.-Sol. Ea.*, 109, B09405, doi:10.1029/2003JB002960, 2004. 1145
- Joughin, I., Bamber, J. L., Scambos, T., Tulaczyk, S., Fahnestock, M., and MacAyeal, D. R.: Integrating satellite observations with modelling: basal shear stress of the Filcher–Ronne ice streams, Antarctica, *Philos. T. R. Soc. A.*, 364, 1795–1814, doi:10.1098/rsta.2006.1799, 2006. 1145
- Joughin, I., Smith, B. E., Howat, I. M., Floricioiu, D., Alley, R. B., Truffer, M., and Fahnestock, M.: Seasonal to decadal scale variations in the surface velocity of Jakobshavn Isbrae, Greenland: Observation and model-based analysis, *J. Geophys. Res.-Earth*, 117, , f02030, doi:10.1029/2011JF002110, 2012. 1145
- Kessler, M. A., Anderson, R. S., and Briner, J. P.: Fjord insertion into continental margins driven by topographic steering of ice, *Nat. Geosci.*, 1, 365–369, 2008. 1145, 1146
- Le Meur, E., Gagliardini, O., Zwinger, T., and Ruokolainen, J.: Glacier flow modelling: a comparison of the Shallow Ice Approximation and the full-Stokes solution, *C. R. Phys.*, 5, 709–722, 2004. 1146, 1147, 1159
- Leith, K., Moore, J. R., Amann, F., and Loew, S.: Subglacial extensional fracture development and implications for Alpine Valley evolution, *J. Geophys. Res.-Earth*, 119, 62–81, doi:10.1002/2012JF002691, 2014. 1161
- MacGregor, K. R., Anderson, R., Anderson, S., and Waddington, E.: Numerical simulations of glacial-valley longitudinal profile evolution, *Geology*, 28, 1031–1034, 2000. 1145, 1146
- MacGregor, K. R., Anderson, R. S., and Waddington, E. D.: Numerical modeling of glacial erosion and headwall processes in alpine valleys, *Geomorphology*, 103, 189–204, 2009. 1145, 1146
- Mahaffy, M. W.: A three-dimensional numerical model of ice sheets: tests on the Barnes Ice Cap, Northwest Territories, *J. Geophys. Res.*, 81, 1059–1066, 1976. 1146
- Morlighem, M., Seroussi, H., Larour, E., and Rignot, E.: Inversion of basal friction in Antarctica using exact and incomplete adjoints of a higher-order model, *J. Geophys. Res.-Earth*, 118, 1746–1753, doi:10.1002/jgrf.20125, 2013. 1145
- Oerlemans, J.: Numerical experiments on large-scale glacial erosion, *Z. Gletscherkunde und Glazialgeologie*, 20, 107–126, 1984. 1145, 1146

The evolution of glacial dynamics

C. F. Brædstrup et al.

Title Page

Abstract

Introduction

Conclusions

References

Tables

Figures



Back

Close

Full Screen / Esc

Printer-friendly Version

Interactive Discussion



- Pattyn, F.: A new three-dimensional higher-order thermomechanical ice sheet model: basic sensitivity, ice stream development, and ice flow across subglacial lakes, *J. Geophys. Res.-Sol. Ea.*, 108, EPM 4–1, doi:10.1029/2002JB002329, 2003. 1146
- Pattyn, F., Perichon, L., Aschwanden, A., Breuer, B., de Smedt, B., Gagliardini, O., Gudmundsson, G. H., Hindmarsh, R. C. A., Hubbard, A., Johnson, J. V., Kleiner, T., Kononov, Y., Martin, C., Payne, A. J., Pollard, D., Price, S., Rückamp, M., Saito, F., Souček, O., Sugiyama, S., and Zwinger, T.: Benchmark experiments for higher-order and full-Stokes ice sheet models (ISMIP–HOM), *The Cryosphere*, 2, 95–108, doi:10.5194/tc-2-95-2008, 2008. 1147
- Pedersen, V. K. and Egholm, D. L.: Glaciations in response to climate variations preconditioned by evolving topography, *Nature*, 493, 206–210, 2013. 1145, 1161
- Pedersen, V. K., Huismans, R. S., Herman, F., and Egholm, D. L.: Controls of initial topography on temporal and spatial patterns of glacial erosion, *Geomorphology*, 223, 96–116, 2014. 1145, 1152
- Pelletier, J. D., Comeau, D., and Kargel, J.: Controls of glacial valley spacing on Earth and Mars, *Geomorphology*, 116, 189–201, 2010. 1144
- Penck, A.: Glacial features in the surface of the Alps, *J. Geol.*, 13, 1–19, 1905. 1144
- Schlunegger, F. and Hinderer, M.: Pleistocene/Holocene climate change, re-establishment of fluvial drainage network and increase in relief in the Swiss Alps, *Terra Nova*, 15, 88–95, 2003. 1161
- Schoof, C.: The effect of cavitation on glacier sliding, *P. Roy. Soc. A-Math. Phys.*, 461, 609–627, doi:10.1098/rspa.2004.1350, 2005. 1151, 1158
- Sedik, H., Sugiyama, S., and Naruse, R.: Numerical simulation of glacial-valley cross-section evolution, *B. Glaciol. Res.*, 22, 75–79, 2005. 1152, 1157, 1160
- Stokes, G. G.: On the theories of the internal friction of fluids in motion and of the equilibrium and motion of elastic solids, *Trans. Cambridge Philos. Soc.*, 8, 287–319, 1845. 1146
- Sugden, D. E. and John, B. S.: *Glaciers and Landscape*, Edward Arnold, London, England, 1976. 1144
- Tomkin, J. H.: Numerically simulating alpine landscapes: the geomorphologic consequences of incorporating glacial erosion in surface process models, *Geomorphology*, 103, 180–188, 2009. 1145, 1146
- Tomkin, J. H. and Braun, J.: The influence of alpine glaciation on the relief of tectonically active mountain belts, *Am. J. Sci.*, 302, 169–190, 2002. 1161
- Weertman, J.: On the sliding of glaciers, *J. Glaciol.*, 3, 33–38, 1957. 1157

Werder, M. A., Hewitt, I. J., Schoof, C. G., and Flowers, G. E.: Modeling channelized and distributed subglacial drainage in two dimensions, *J. Geophys. Res.-Earth*, 118, 2140–2158, 2013. 1151

ESURFD

3, 1143–1178, 2015

The evolution of glacial dynamics

C. F. Brædstrup et al.

Title Page

Abstract

Introduction

Conclusions

References

Tables

Figures



Back

Close

Full Screen / Esc

Printer-friendly Version

Interactive Discussion



The evolution of glacial dynamics

C. F. Brædstrup et al.

Table 1. Model parameters used for all experiments.

Parameters		Value unit
ρ_i	Ice Density	910.0 kg m ⁻³
dT_h	Atmospheric lapse rate	6.0 °C km ⁻¹
g	Acceleration of gravity	9.82 m s ⁻²
A	Ice flow parameter	1×10^{-16} Pa ⁻³ yr ⁻¹
n	Ice flow stress exponent	3
C_s	Weertman sliding coefficient	2×10^{-9} m Pa ⁻² yr ⁻¹
C_s	Empirical sliding coefficient	2×10^{-3} m Pa ⁻¹ yr ⁻¹
C_s	Columb-friction sliding coefficient	0.25
λ_0	Columb-friction sliding parameter	2×10^{-17} m Pa ⁻³ yr ⁻¹
m_{acc}	Accumulation gradient	0.5 m yr ⁻¹ °C ⁻¹
m_{alb}	Ablation gradient	1.5 m yr ⁻¹ °C ⁻¹
T_{sl}	Sea-level temperature	6 °C
K_a	Subglacial abrasion erosion constant	2.5×10^{-6} m ⁻¹ yr ⁻¹
m	Subglacial erosion exponent	1–2

[Title Page](#)
[Abstract](#)
[Introduction](#)
[Conclusions](#)
[References](#)
[Tables](#)
[Figures](#)
[Back](#)
[Close](#)
[Full Screen / Esc](#)
[Printer-friendly Version](#)
[Interactive Discussion](#)


The evolution of glacial dynamics

C. F. Brædstrup et al.

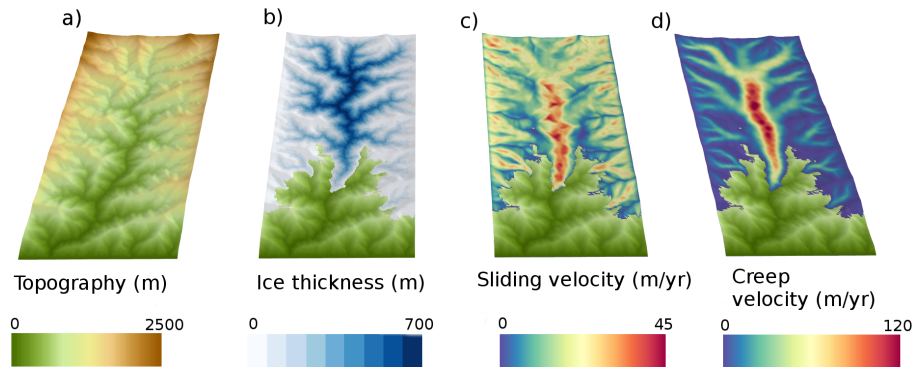


Figure 1. Bed topography **(a)**, steady-state ice thickness **(b)**, sliding velocity **(c)**, and depth-averaged creep velocity **(d)** for experiment 1. The velocities shown are from iSOSIA.

[Title Page](#)[Abstract](#)[Introduction](#)[Conclusions](#)[References](#)[Tables](#)[Figures](#)[Back](#)[Close](#)[Full Screen / Esc](#)[Printer-friendly Version](#)[Interactive Discussion](#)

The evolution of glacial dynamics

C. F. Brædstrup et al.

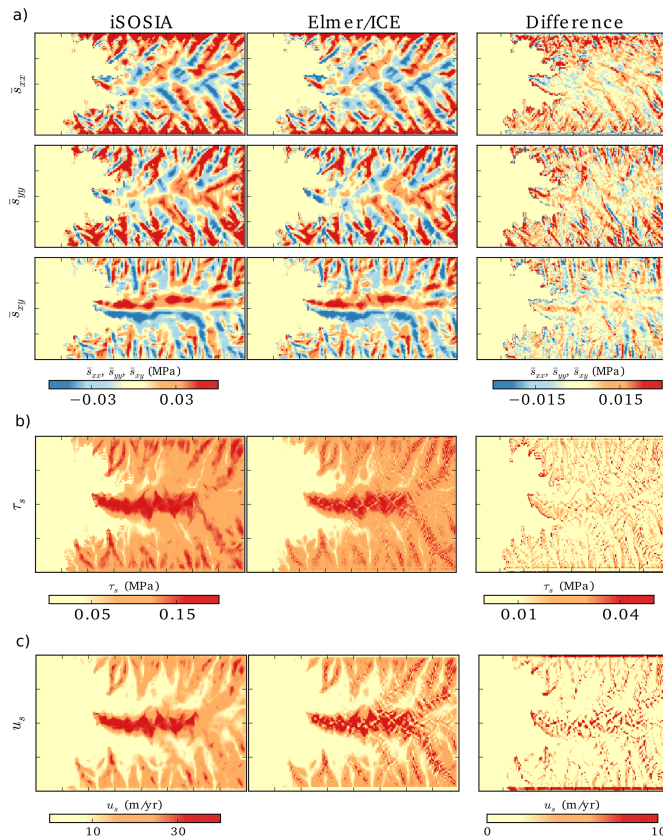


Figure 2. (a) Comparison of stress components from iSOSIA and Elmer/ICE shown in top view. The first two columns show the depth-averaged stress components \bar{s}_{xx} , \bar{s}_{yy} , and \bar{s}_{xy} . The right-most column shows the difference between iSOSIA and Elmer/ICE results. (b) Basal shear stress for both models. (c) Sliding velocity using a Weertman relation (Eq. 6). Ice flow is from right to left.

Title Page

Abstract

Introduction

Conclusions

References

Tables

Figures

◀

▶

◀

▶

Back

Close

Full Screen / Esc

Printer-friendly Version

Interactive Discussion



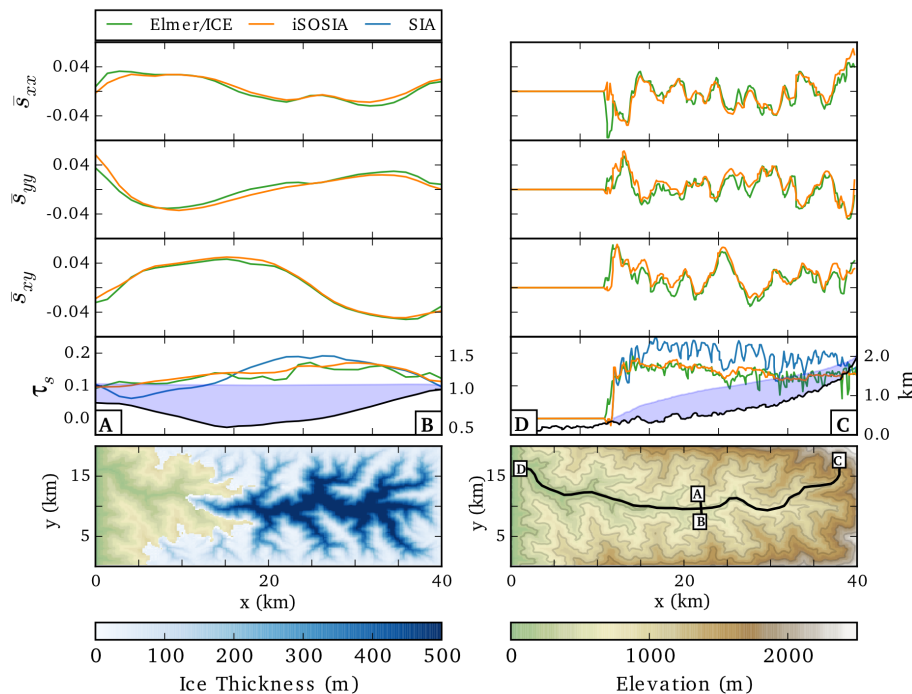


Figure 3. iSOSIA (orange) and Elmer/ICE (green) stress components along a transverse (left column) and a longitudinal (right column) profile in MPa. Upper three rows compare the higher-order horizontal stress components. The fourth row shows the basal shear stress along the same profiles. The SIA driving stress (Eq. 15) is also shown for comparison (blue line). The fourth row also shows bed topography (black line) and ice thickness (blue shaded area). Notice that elevation is indicated on right axis. Bottom left panel shows ice thickness. The position of the two profiles (A–B and C–D) are shown in the bottom right panel.

Title Page

Abstract

Introduction

Conclusions

References

Tables

Figures

◀

▶

◀

▶

Back

Close

Full Screen / Esc

Printer-friendly Version

Interactive Discussion



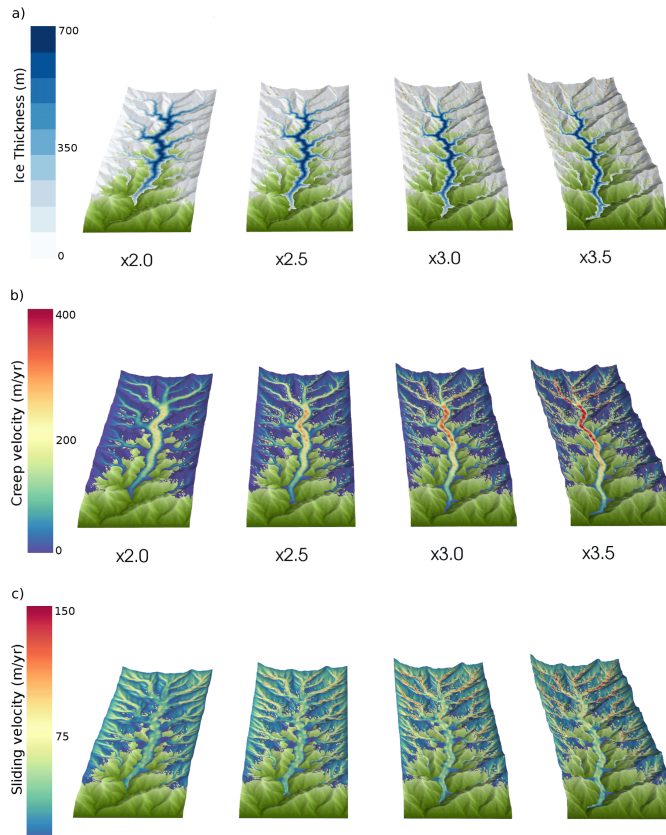


Figure 4. Bed topography with ice cover (a), creep velocity (b), and basal sliding velocity (c) computed at steady-state using iSOSIA for the four scaling factors in experiment 2. The total relief is 3750, 5000, 6250, and 7500 m respectively.

Title Page

Abstract

Introduction

Conclusions

References

Tables

Figures



Back

Close

Full Screen / Esc

Printer-friendly Version

Interactive Discussion



Title Page

Abstract

Introduction

Conclusions

References

Tables

Figures



Back

Close

Full Screen / Esc

Printer-friendly Version

Interactive Discussion

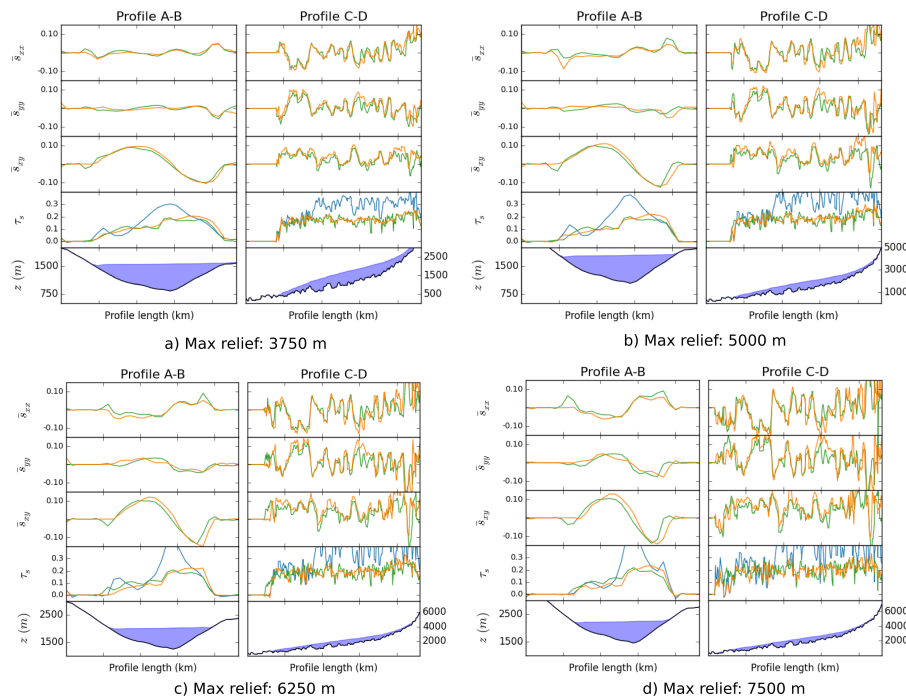


Figure 5. Stress components in MPa from iSOSIA (orange) and Elmer/ICE (green) for the increasing topographical relief in experiment 2. Left column of each panel (**a–d**) shows values along the transverse profile A–B, while the right column is along the longitudinal profile C–D (Fig. 3). The SIA driving stress approximation is also shown in the third row for comparison (blue line). Forth row shows the ice-surface and bed topography along the same profiles. Note that elevation is indicated on the left and right axis respectively.

The evolution of glacial dynamics

C. F. Brædstrup et al.

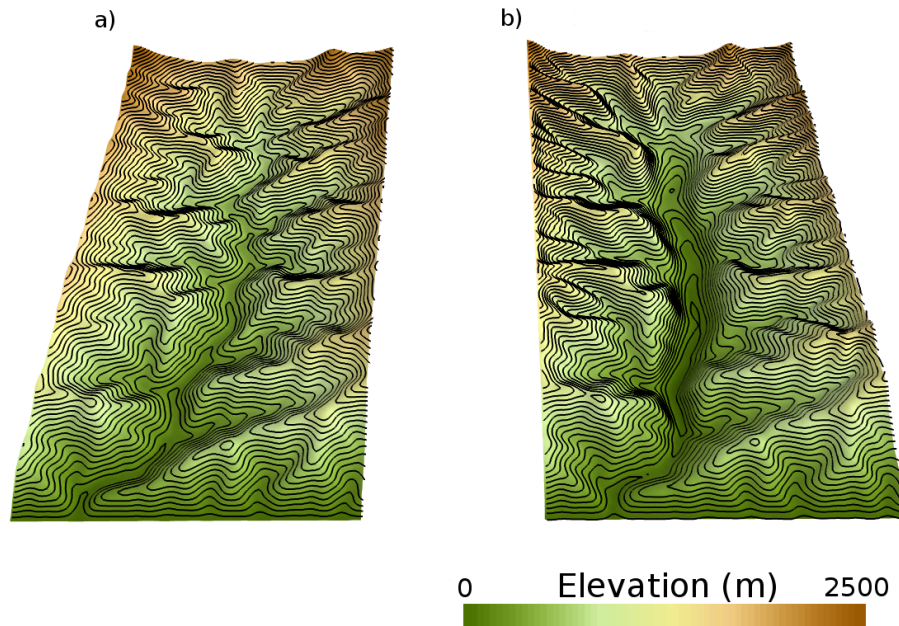


Figure 6. Preglacial landscape showing the initial fluvial topography **(a)**. The postglacial landscape after 100 m of average erosion (using $m = 2$ in Eq. 9). **(b)**. Several characteristic features of glaciated landscapes are evident in **(b)**. The trunk valley is widened with steep slopes along the sides forming a U-shaped cross section. Flattened valley floors, hanging valleys and truncated spurs are also visible.

The evolution of glacial dynamics

C. F. Brædstrup et al.

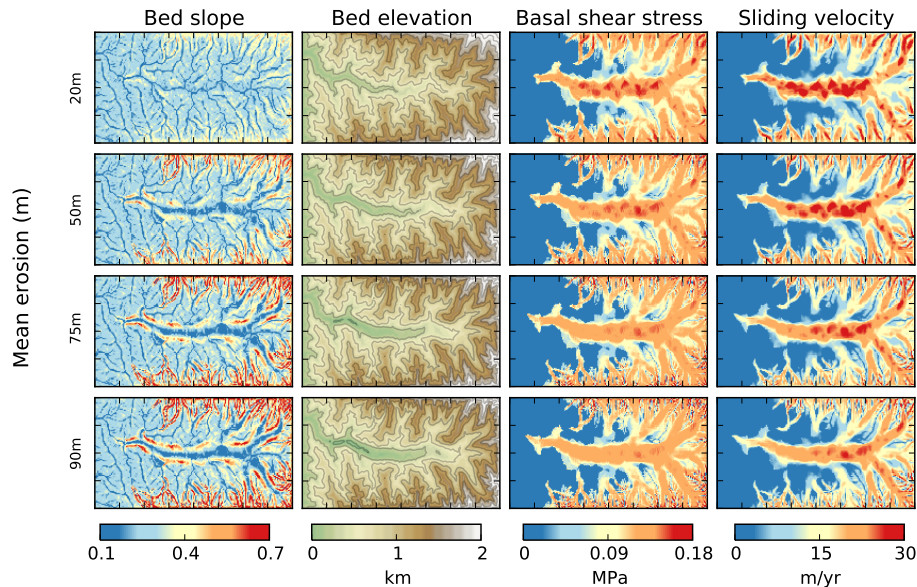


Figure 7. The results from experiment 3 with glacial erosion and using the Weertman sliding relation (Eq. 6) and $m = 2$ in Eq. (9). Each column shows bed slope, bed elevation, basal shear stress and basal sliding speed at different stages of erosion.

Title Page

Abstract

Introduction

Conclusions

References

Tables

Figures



Back

Close

Full Screen / Esc

Printer-friendly Version

Interactive Discussion



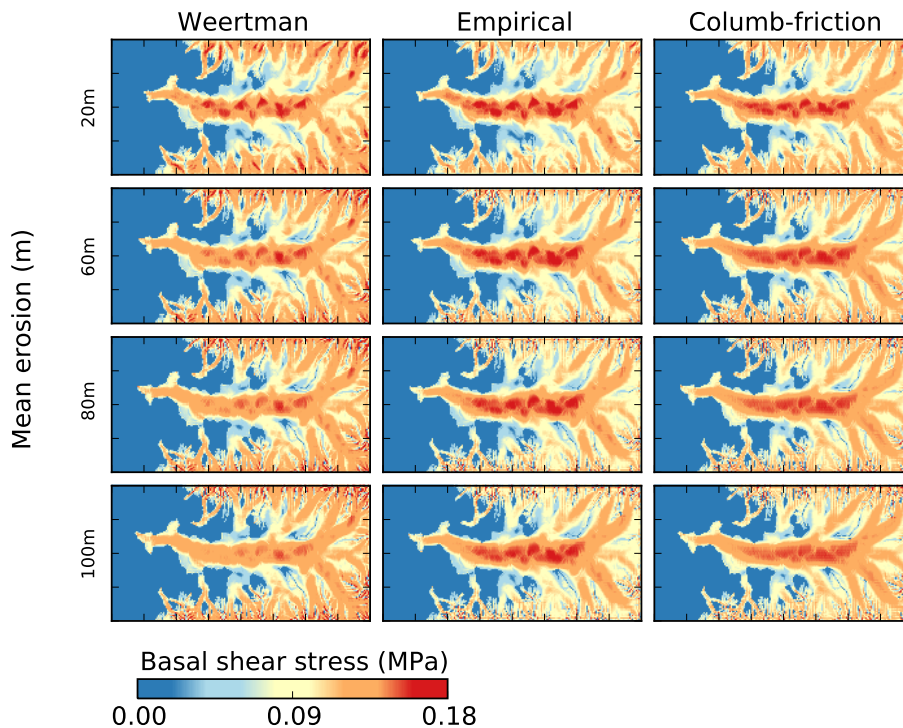


Figure 8. Results from experiment 3 using different sliding relations and $m = 2$ in Eq. (9). The three columns show basal shear stress for the different sliding laws: Weertman (Eq. 6), empirical (Eq. 7) and Columb-friction (Eq. 8) at different stages of glacial erosion.

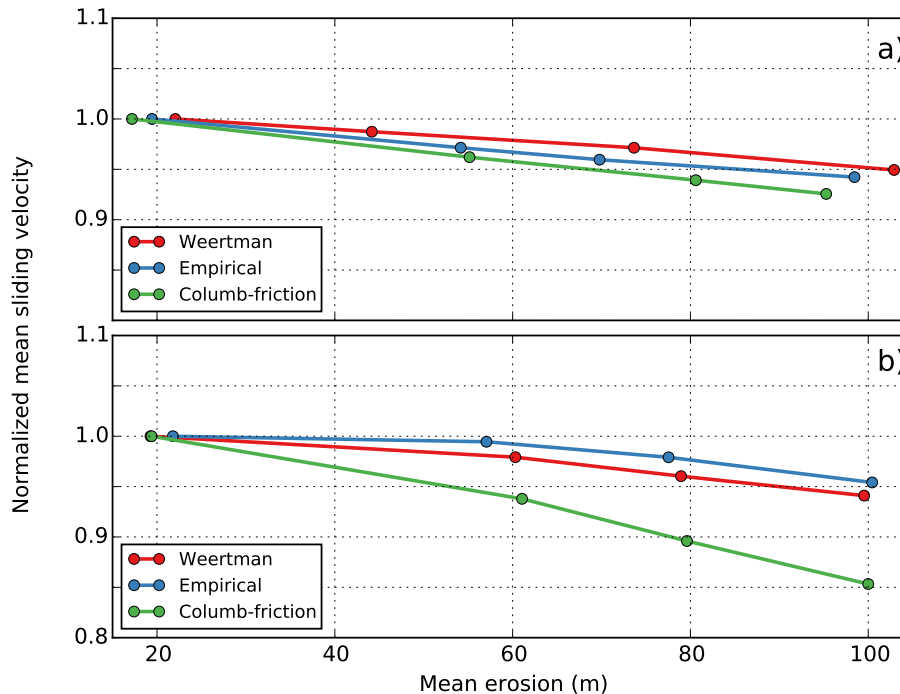


Figure 9. Evolution of normalised mean sliding rate as a function of mean erosion for three different sliding laws. **(a)** Shows results using a linear erosion law ($m = 1$ in Eq. 9). **(b)** Results using $m = 2$. The means of sliding rate and erosion are computed only for the trunk valley, defined as all glaciated cells below 750 m elevation in the initial fluvial landscape.